



CHORUS

This is the accepted manuscript made available via CHORUS. The article has been published as:

Flexocaloric effect near a ferroelastic transition

Marcel Porta, Teresa Castán, Avadh Saxena, and Antoni Planes

Phys. Rev. B **104**, 094108 — Published 24 September 2021

DOI: [10.1103/PhysRevB.104.094108](https://doi.org/10.1103/PhysRevB.104.094108)

Flexocaloric effect near a ferroelastic transition

Marcel Porta,¹ Teresa Castán,² Avadh Saxena,³ and Antoni Planes²

¹*Departament de Física Quàntica i Astrofísica, Facultat de Física, Universitat de Barcelona, Martí i Franquès 1, 08028 Barcelona, Catalonia.*

²*Departament de Física de la Matèria Condensada, Facultat de Física, Universitat de Barcelona, Martí i Franquès 1, 08028 Barcelona, Catalonia.*

³*Theoretical Division, Los Alamos National Laboratory, Los Alamos, NM 87545, USA.*

A Ginzburg-Landau model embedded into a vibrational model is used to study the flexocaloric effect in a beam near a ferroelastic transition. The caloric response upon bending is characterized by the isothermal entropy change and the adiabatic temperature change of the beam. We obtain a larger response relative to the strength of the applied forces at temperatures slightly above the transition temperature. It is also obtained that the maximum caloric response is almost linear with the bending angle of the beam whereas the relation between the bending angle and the applied forces is highly nonlinear. Small hysteresis associated with the phase transition is obtained for sufficiently large bending forces due to the existence of a critical point in the temperature-stress phase diagram of the ferroelastic material. Finally, the microstructure changes with bending in the beam are consistent with previous experimental observations.

I. INTRODUCTION

In recent years there has been a great deal of interest in developing environmentally friendly cooling techniques that can efficiently replace the current technology based on vapor compression, which uses fluids with strong global warming adverse effects. Among the different possibilities, solid state technologies, based on materials exhibiting giant caloric effects, are nowadays considered the most promising¹.

Caloric effects rely on the reversible thermal response of solid materials to changes induced by an externally applied field, either electric, magnetic or mechanical. The corresponding effects are denoted as electro-, magneto- and mechanocaloric effects, respectively. The caloric response is in general quantified by either the change of entropy induced by isothermal application of the field or the change of temperature that occurs when the field is applied or removed adiabatically². A number of ferroic (and multiferroic) materials display very large caloric effects close to the phase transition where the relevant ferroic property spontaneously emerges. Particularly interesting are first order transitions which can be induced by externally applied fields with an associated large latent heat^{1,3,4}. This is the class of materials that has been acknowledged to be potentially interesting for solid state cooling and energy harvesting applications⁵.

Among the caloric materials, mechanocaloric materials have opened up excellent promise for applications^{6,7}. In this class of materials caloric effects are usually induced by uniaxial stress or by hydrostatic pressure. However, in practical applications flexion, bending or twisting is a very convenient stress mode since it is much easily implemented in refrigeration or harvesting devices⁸, the required force decreases at the expense of increased displacement^{9,10}, and has the advantage of localizing the areas where large changes of temperature may occur. In addition, the large surface to volume ratio of thin beams or fibers is conducive to efficient heat transfer. Com-

pared with the homogeneous deformation induced by uniaxial stress or hydrostatic pressure, bending or twisting induces stress gradients strongly concentrated in the regions of maximum curvature. The caloric effect associated with the application of a field that couples to the gradient of the strain is known as the flexocaloric effect. In a broader context, caloric effects associated with bending or twisting a material are also known as flexocaloric as these deformation modes involve large strain gradients.

Recently there has been an incipient interest in studying the caloric response of materials subjected to inhomogeneous stress modes. Specifically, the caloric response of NiTi shape-memory alloy, rubber and plastic fibers¹⁰⁻¹² subjected to bending or twisting has been demonstrated. Nevertheless, studies dealing with the thermodynamics of mechanocaloric materials subjected to inhomogeneous stress modes are still scarce. In the present paper we propose a model for a ferroelastic transition that is adequate for studying flexocaloric effects in the vicinity of the ferroelastic transition. The model is formulated in two dimensions for a system undergoing a square-to-rectangle transition, that can be considered as the analogue of a three-dimensional (3D) cubic-to-tetragonal transition, commonly occurring among many ferroelastics. In fact, the former can be conceived as the cross-section of the latter and, therefore, the obtained results are expected to be meaningful for the study of flexocaloric effects in a variety of real materials.

Actually, the present study represents a first step in the quest for new caloric materials since, as it is well known, in some materials strain gradients can induce strong polar and magnetic response¹³, which suggests that the combined application of flexion and electric or magnetic fields in this class of materials might be a very convenient strategy to induce an enhanced multicaloric response¹⁴. Additionally, it would be worthwhile to explore caloric effects in flexoelectric¹⁵⁻¹⁷, flexomagnetic¹⁸ and flexomagnetoelectric^{19,20} materials.

The paper is organized as follows. In Sec. II we intro-

duce the model, a strain based free energy and the corresponding dynamical equations. The elastic and thermodynamic properties obtained from the model for a bent (ferroelastic) beam are presented in Sec. III. The change in microstructure is found to be consistent with experimental observations²¹. Finally, in Sec. IV we summarize our main results and draw specific conclusions.

II. MODEL

In this section we present a mesoscopic model for a ferroelastic material as the constituent of a two-dimensional (2D) macroscopic beam of size $L_x \times L_y$ with free boundary conditions [Fig. 1(a)]. The beam is considered to be

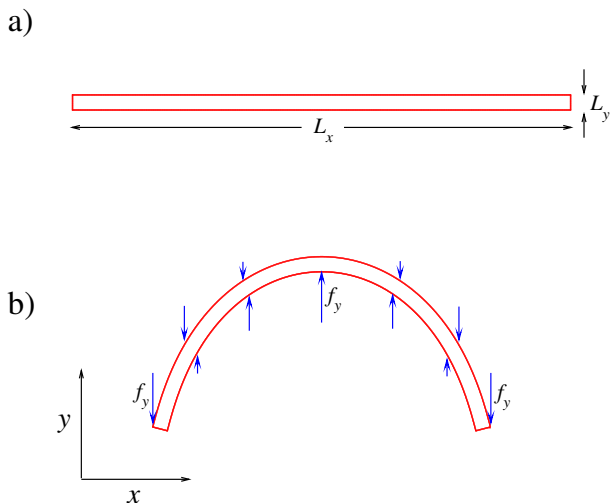


FIG. 1: (a) Beam of size $L_x \times L_y$ in the absence of external forces, and (b) with applied external forces, f_y .

the projection onto a 2D space of a 3D sheet of width L_x , thickness L_y and with no boundaries in z direction. Thus, all results will be given per unit length in z direction, assuming that all physical variables describing the beam are constant along this direction.

The Helmholtz free energy of the beam is written as the free energy of a set of $3N$ classical harmonic oscillators with frequency ω_i which are the building blocks of the 3D sheet,

$$\mathcal{F}_{vib} = k_B T \sum_{i=1}^{3N} \ln \left(\frac{\hbar \omega_i}{k_B T} \right). \quad (1)$$

This free energy is divided into two terms,

$$\mathcal{F}_{vib} = \mathcal{F}_\omega + \mathcal{F}_T, \quad (2)$$

the first term, \mathcal{F}_ω , containing the dependence of the vibrational free energy on the frequencies of the oscillators, and the second term, \mathcal{F}_T , that depends on temperature

only,

$$\mathcal{F}_\omega = k_B T \sum_{i=1}^{3N} \ln \left(\frac{\hbar \omega_i}{U} \right), \quad (3)$$

$$\mathcal{F}_T = -3N k_B T \ln \left(\frac{k_B T}{U} \right),$$

where U is the reduced unit of energy. The free energy term \mathcal{F}_ω is modeled using a Ginzburg-Landau expansion in the components of the strain tensor. To this end, the beam is discretized onto a $N_x \times N_y = 1024 \times 32$ mesh.

The distortion of the beam is described by the displacement field,

$$\mathbf{u}(\mathbf{X}) = \mathbf{x}(\mathbf{X}) - \mathbf{X}, \quad (4)$$

where \mathbf{X} are the positions of the cells of the discretized beam in the undistorted or reference configuration, and \mathbf{x} are their positions in the distorted state. These displacement fields, which are the variables of the model, are used to compute the Lagrangian strain field,

$$\varepsilon_{ij}(\mathbf{X}) = \frac{1}{2} \left(\frac{\partial u_i}{\partial X_j} + \frac{\partial u_j}{\partial X_i} + \sum_k \frac{\partial u_k}{\partial X_i} \frac{\partial u_k}{\partial X_j} \right), \quad (5)$$

which in turn will be used to compute the elastic free energy, \mathcal{F}_ω .

The beam is a single crystal of a ferroelastic material with a square-to-rectangle phase transition that can be bent by applying external forces. The order parameter (OP) of the transformation, which is of first order, is the deviatoric strain, $e_2 = (\varepsilon_{xx} - \varepsilon_{yy})/\sqrt{2}$. Thus, the Ginzburg-Landau expansion of the free energy density is written up to sixth order in the OP. In addition, we include the lowest order contribution of the non-OP components of the strain tensor, dilatation $e_1 = (\varepsilon_{xx} + \varepsilon_{yy})/\sqrt{2}$ and shear $e_3 = \varepsilon_{xy}$, which play an important role in heterogeneous strain configurations, and the lowest order contribution of the gradient of all strain components,

$$f_\omega \approx \frac{1}{2} A (T - T_c) e_2^2 + \frac{1}{4} \beta e_2^4 + \frac{1}{6} \gamma e_2^6 + \frac{1}{2} A_1 e_1^2 + \frac{1}{2} A_3 e_3^2 + \frac{1}{2} \kappa_1 |\nabla e_1|^2 + \frac{1}{2} \kappa_2 |\nabla e_2|^2 + \frac{1}{2} \kappa_3 |\nabla e_3|^2, \quad (6)$$

where T is the temperature and T_c is the stability limit of the square phase. In summary, the free energy term \mathcal{F}_ω in Eq. (3) is evaluated as,

$$\mathcal{F}_\omega = \int f_\omega d\mathbf{X}, \quad (7)$$

with f_ω given by Eq. (6). The temperature dependence of the free energy is thus limited to the quadratic term in the Landau free energy density and to the free energy term \mathcal{F}_T . We also note that f_ω includes physical nonlinearities (fourth and sixth order elastic constants) and thus, the phonon frequencies in Eq. (3) need to be interpreted as being effective and temperature dependent in an anharmonic system.

An efficient and simple way of obtaining the equilibrium state of the beam under an applied external force is by solving the dynamical equations of the displacement field,

$$\rho \ddot{u}_i = \rho g_i + \sum_j \frac{\partial \sigma_{ij}}{\partial x_j}, \quad (8)$$

where the dots stand for time derivative, ρ is the density of the deformed configuration, g_i is the i -th component of an external force (per unit mass), σ_{ij} are the components of the Cauchy stress tensor, and we recall that x_j is the j -th component of the position vector of a unit cell of the discretized beam in the deformed configuration. Using more appropriate variables the dynamical equations can be written as²²,

$$\rho_0 \ddot{u}_i = \rho_0 g_i + \sum_j \frac{\partial \tau_{ij}}{\partial X_j}, \quad (9)$$

where ρ_0 is the density of the undistorted beam, τ_{ij} are the components of the first Piola-Kirchhoff stress tensor and X_j is the j -th component of the position vector of a unit cell of the discretized beam in the reference configuration. The first Piola-Kirchhoff stress tensor is the work conjugate of the deformation gradient, F_{ij} , defined as,

$$F_{ij} = \frac{\partial x_i}{\partial X_j} = \frac{\partial u_i}{\partial X_j} + \delta_{ij} = d_{ij} + \delta_{ij}, \quad (10)$$

where we define,

$$d_{ij} = \frac{\partial u_i}{\partial X_j}. \quad (11)$$

Thus, using the chain rule the first Piola-Kirchhoff stress tensor can be obtained from the Helmholtz free energy,

$$\tau_{ij} = \frac{\delta \mathcal{F}_{vib}}{\delta F_{ij}} = \sum_{m=1}^3 \frac{\delta \mathcal{F}_\omega}{\delta e_m} \frac{\partial e_m}{\partial F_{ij}}, \quad (12)$$

where the free energy,

$$\mathcal{F}_\omega = \int f_\omega(e_m, \partial e_m / \partial X_i) d\mathbf{X}, \quad (13)$$

is a functional of the strain fields and the strain gradients. Thus we have,

$$\tau_{ij} = \sum_{m=1}^3 \left(\frac{\partial f_\omega}{\partial e_m} - \sum_k \frac{\partial}{\partial X_k} \frac{\partial f_\omega}{\partial (\partial e_m / \partial X_k)} \right) \frac{\partial e_m}{\partial F_{ij}}, \quad (14)$$

which yields,

$$\begin{aligned} \tau_{xx} &= [A(T - T_c)e_2 + \beta e_2^3 + \gamma e_2^5 + A_1 e_1] \\ &\quad \times \frac{1}{\sqrt{2}}(1 + d_{xx}) + A_3 e_3 \frac{1}{2} d_{xy} - (\kappa_1 \nabla^2 e_1 + \kappa_2 \nabla^2 e_2) \\ &\quad \times \frac{1}{\sqrt{2}}(1 + d_{xx}) - \kappa_3 (\nabla^2 e_3) \frac{1}{2} d_{xy}, \\ \tau_{xy} &= [- (A(T - T_c)e_2 + \beta e_2^3 + \gamma e_2^5) + A_1 e_1] \\ &\quad \times \frac{1}{\sqrt{2}} d_{xy} + A_3 e_3 \frac{1}{2} (1 + d_{xx}) - (\kappa_1 \nabla^2 e_1 - \kappa_2 \nabla^2 e_2) \\ &\quad \times \frac{1}{\sqrt{2}} d_{xy} - \kappa_3 (\nabla^2 e_3) \frac{1}{2} (1 + d_{xx}), \\ \tau_{yx} &= [A(T - T_c)e_2 + \beta e_2^3 + \gamma e_2^5 + A_1 e_1] \frac{1}{\sqrt{2}} d_{yx} \\ &\quad + A_3 e_3 \frac{1}{2} (1 + d_{yy}) - (\kappa_1 \nabla^2 e_1 + \kappa_2 \nabla^2 e_2) \frac{1}{\sqrt{2}} d_{yx} \\ &\quad - \kappa_3 (\nabla^2 e_3) \frac{1}{2} (1 + d_{yy}), \\ \tau_{yy} &= [- (A(T - T_c)e_2 + \beta e_2^3 + \gamma e_2^5) + A_1 e_1] \\ &\quad \times \frac{1}{\sqrt{2}} (1 + d_{yy}) + A_3 e_3 \frac{1}{2} d_{yx} - (\kappa_1 \nabla^2 e_1 - \kappa_2 \nabla^2 e_2) \\ &\quad \times \frac{1}{\sqrt{2}} (1 + d_{yy}) - \kappa_3 (\nabla^2 e_3) \frac{1}{2} d_{yx}. \end{aligned} \quad (15)$$

In geometrically linear elasticity the stress tensor is sometimes defined as the partial derivative of the free energy density with respect to the linear strain tensor, and the partial derivative of the free energy density with respect to the strain gradient is referred to as the hyperstress or the double stress²³. In this case, the functional derivative of the free energy with respect to the linear strain tensor, which is a combination of the stress and the hyperstress is referred to as the total stress. In the present work we introduce the first Piola-Kirchhoff stress tensor as the functional derivative of the free energy with respect to the deformation gradient. Thus, this definition corresponds to the total stress and contains the dependence of the free energy density on both the strain and the strain gradients. Consequently, the divergence of the first Piola-Kirchhoff stress tensor yields the total elastic force in a volume element of the beam.

To dissipate the excess free energy of the beam during its relaxation to equilibrium we introduce the Rayleigh potential,

$$R = \frac{1}{2} \sum_{m=1}^3 \bar{A}_m \dot{e}_m^2, \quad (16)$$

which yields the damping stress tensor,

$$\bar{\tau}_{ij} = \frac{\delta}{\delta \dot{F}_{ij}} \int R d\mathbf{X} = \frac{\partial R}{\partial \dot{F}_{ij}}, \quad (17)$$

and the associated damping force,

$$h_i = \frac{1}{\rho_0} \sum_j \frac{\partial \bar{\tau}_{ij}}{\partial X_j}. \quad (18)$$

Applying the chain rule the damping stresses are,

$$\begin{aligned}\bar{\tau}_{xx} &= (\bar{A}_1 \dot{\epsilon}_1 + \bar{A}_2 \dot{\epsilon}_2) \frac{1}{\sqrt{2}}(1 + d_{xx}) + \bar{A}_3 \dot{\epsilon}_3 \frac{1}{2} d_{xy}, \\ \bar{\tau}_{xy} &= (\bar{A}_1 \dot{\epsilon}_1 - \bar{A}_2 \dot{\epsilon}_2) \frac{1}{\sqrt{2}} d_{xy} + \bar{A}_3 \dot{\epsilon}_3 \frac{1}{2} (1 + d_{xx}), \\ \bar{\tau}_{yx} &= (\bar{A}_1 \dot{\epsilon}_1 + \bar{A}_2 \dot{\epsilon}_2) \frac{1}{\sqrt{2}} d_{yx} + \bar{A}_3 \dot{\epsilon}_3 \frac{1}{2} (1 + d_{yy}), \\ \bar{\tau}_{yy} &= (\bar{A}_1 \dot{\epsilon}_1 - \bar{A}_2 \dot{\epsilon}_2) \frac{1}{\sqrt{2}}(1 + d_{yy}) + \bar{A}_3 \dot{\epsilon}_3 \frac{1}{2} d_{yx}.\end{aligned}\quad (19)$$

Finally, to bend the beam we apply a distribution of external forces to its long edge that vary linearly with the position where they are applied, as shown schematically in Fig. 1(b). Analytically the forces are given by the expression,

$$\begin{aligned}f_y(X, Y = 0) &= \begin{cases} 2f_0 X/L_x, & X \leq L_x/2 \\ 2f_0 - 2f_0 X/L_x, & X > L_x/2, \end{cases} \\ f_y(X, Y = L_y) &= \begin{cases} -f_0 + 2f_0 X/L_x, & X \leq L_x/2 \\ f_0 - 2f_0 X/L_x, & X > L_x/2, \end{cases}\end{aligned}\quad (20)$$

where $X = X_x$, $Y = X_y$, and f_0 is a parameter.

Expanding Eq. (9) and taking into account the damping force as an external force we obtain,

$$\begin{aligned}\rho_0 \ddot{u}_x &= \frac{\partial(\tau_{xx} + \bar{\tau}_{xx})}{\partial X} + \frac{\partial(\tau_{xy} + \bar{\tau}_{xy})}{\partial Y}, \\ \rho_0 \ddot{u}_y &= \rho_0 f_y + \frac{\partial(\tau_{yx} + \bar{\tau}_{yx})}{\partial X} + \frac{\partial(\tau_{yy} + \bar{\tau}_{yy})}{\partial Y},\end{aligned}\quad (21)$$

where the first Piola-Kirchhoff stress tensor is given by Eq. (15), the damping stress tensor is given by Eq. (19), and the external forces that are applied to bend the beam are given in Eq. (20).

Equation (21) is integrated using the leap-frog Verlet algorithm²⁴. As the damping force in a volume element of the beam is written as the divergence of a damping stress tensor, the friction force is large for short wavelength oscillations of the beam, but is inefficient to dissipate the energy associated with long wavelength distortions. Thus, to reach the equilibrium configurations in reasonably short times, every $10^4 - 10^5$ integration time steps the velocity of all volume elements of the beam is set to zero.

The parameters A , T_c , κ_2 and ρ_0 are set to unity, which define reduced units of length, energy, mass and temperature. Some other parameters are taken from a fit to Fe-Pd by Kartha *et al.*²⁵, and in reduced units are $\beta = -2.76 \times 10^2$, $\gamma = 4.86 \times 10^5$, $A_1 = 2.27$, and $A_3 = 4.54$. The remaining model parameters are $\kappa_1 = \kappa_3 = 1$ and $\bar{A}_1 = \bar{A}_2 = \bar{A}_3 = 0.2$. The size of the beam is $L_x \times L_y = 2000 \times 62.5$ (in reduced units) which leads to a number of oscillators per unit length in Fe-Pd of $3N = 3.746 \times 10^5$, where we have used that Fe-Pd has an fcc crystal structure with lattice parameter²⁶ $a = 0.3758$ nm. With these model parameters the square-to-rectangle phase transition in the absence of applied forces occurs at $T_0 = T_c + 3\beta^2/16A\gamma = 1.029T_c$.

III. ELASTIC AND THERMODYNAMIC PROPERTIES OF THE BENT BEAM

In this section we present the elastic and thermodynamic properties of the beam obtained from fully relaxed static configurations. In Fig. 2 we show the shape of the beam obtained at $T = 1.05T_c$, above the transition temperature, for five different values of the parameter f_0 which controls the strength of the applied forces. The corresponding OP deviatoric strain field is also plotted using a gray scale, where gray stands for the high temperature square phase and white/black stand for the two variants of the rectangular phase. The nucleation of the rectangular phase induced by stress is obtained in the curved regions of the beam, the horizontal variant nucleating in the stretched external part of the curved regions, and the vertical variant nucleating in the compressed internal part of the curved regions, as shown schematically.

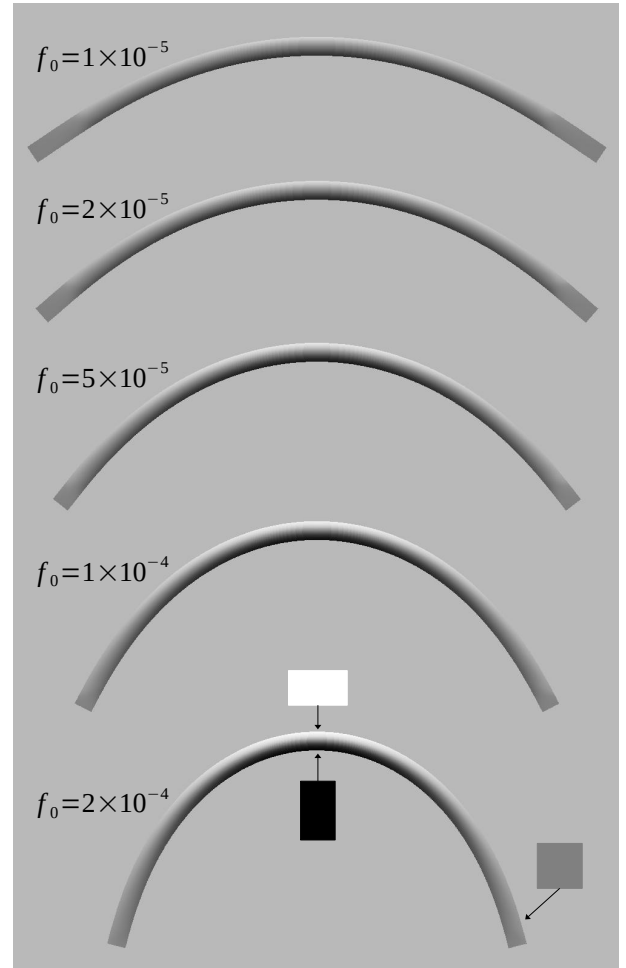


FIG. 2: Bent beam at $T = 1.05T_c$ for several values of the parameter f_0 , which controls the strength of the distribution of applied forces. The corresponding deviatoric strain field is shown using a gray scale, where gray stands for the square phase and white/black stand for the two variants of the rectangular phase, as shown schematically.

A macroscopic or integral quantity that characterizes the deformation of the beam is the bending angle. This is defined as the change of the angle between the directions where the ends of the beam point when the external forces are applied. The bending angle as a function of the strength of the applied forces is shown in Fig. 3 at three different temperatures above T_0 . The relation obtained

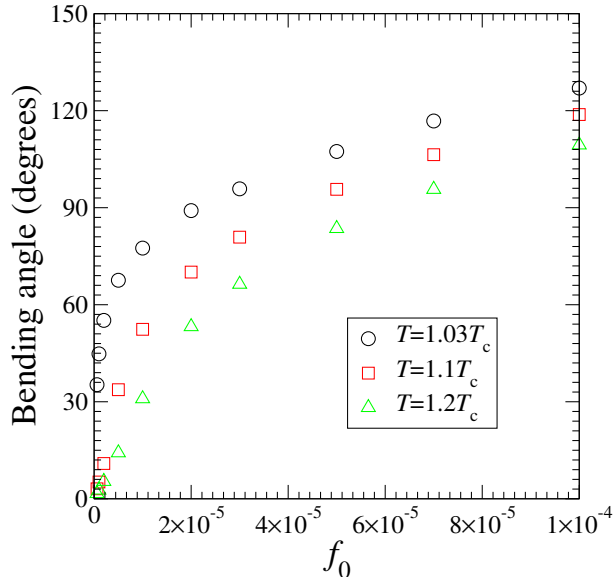


FIG. 3: Bending angle of the beam vs the strength of the distribution of applied forces at three different temperatures.

is highly nonlinear. In addition, the strength of the applied forces that is needed to bend the beam by a given angle decreases as the transition temperature, T_0 , is approached. This is a consequence of the softening of the elastic constant $C' = (C_{11} - C_{12})/2 = A(T - T_c)/2$.

In Fig. 4 we show the bent beam and the corresponding OP deviatoric strain field at different temperatures for $f_0 = 5 \times 10^{-5}$. In this case, below the transition temperature there is a competition between the stress and temperature to induce the rectangular phase. If the effect of the stress is larger than the effect of temperature, we obtain a strain configuration similar to the one obtained above T_0 , with one variant of the rectangular phase nucleating in the external part of the curved regions and the other variant nucleating in the internal part. However, when the effect of temperature dominates over the stress we obtain a twin microstructure with twin boundaries oriented along $\langle 11 \rangle$ directions in order to minimize the elastic energy, which results in a zig-zag microstructure. Still, to accommodate the stress in this microstructure, one of the variants of the rectangular phase is dominant in the external part of the curved regions of the beam and the other variant is dominant in the internal part. These results are consistent with the experimental observation of microstructure changes associated with bending²¹ in CuAlNi.

Given the equilibrium displacement field of the bent

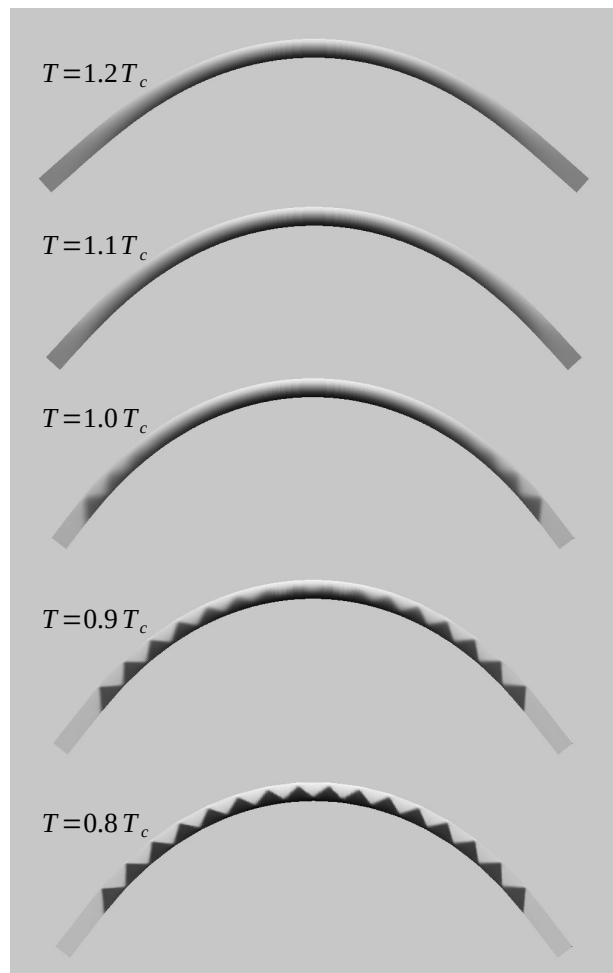


FIG. 4: Bent beam at several temperatures under an external force distribution with $f_0 = 5 \times 10^{-5}$. The corresponding deviatoric strain field is shown using a gray scale, as in Fig. 2.

beam, its entropy is obtained as,

$$S = -\frac{\partial \mathcal{F}_{vib}}{\partial T} = -\frac{A}{2} \int e_2^2 d\mathbf{X} + 3Nk_B \left[1 + \ln \left(\frac{k_B T}{U} \right) \right]. \quad (22)$$

In Fig. 5 we plot the entropy of the beam as a function of temperature for several values of f_0 . The results are given relative to the entropy at $T = 1.5T_c$ in the absence of applied forces. In the absence of external forces the entropy curve is discontinuous due to the first order character of the phase transition. However, in the whole range of applied forces we have used the entropy curve is continuous within numerical precision. This is related to the existence of a critical point in the temperature-stress phase diagram of the model, where the square-to-rectangle phase transition ends. The existence of a critical point has been observed experimentally in Fe-31.2Pd (at. %) and is expected to exist in materials where the transformation strain has a strong dependence on the applied stress²⁷. Nonhysteretic superelasticity similar to

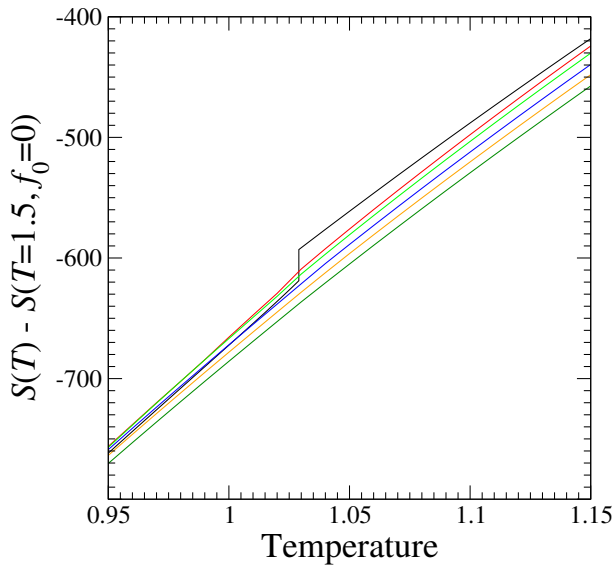


FIG. 5: Entropy of a bent beam vs temperature for $f_0 = 0, 1 \times 10^{-5}, 2 \times 10^{-5}, 5 \times 10^{-5}, 1 \times 10^{-4},$ and 2×10^{-4} (from top to bottom above T_0). Results are given with respect to the entropy at $T=1.5T_c$ in the absence of applied forces.

the one expected above a critical point has also been observed in NiCoFeGa²⁸.

Using a Gibbs free energy density $f = f_w - e_2 \sigma_2$ where $\sigma_2 = (\sigma_{xx} - \sigma_{yy})/\sqrt{2}$ is the deviatoric stress, we have determined that in the model the critical point is located at $T_{\text{cri}} = 1.070T_c$ and $\sigma_2^{\text{cri}} = 4.89 \times 10^{-4}$ in reduced units. Strictly speaking, the work conjugate of the Lagrangian strain tensor is the second Piola-Kirchhoff stress tensor. However, we will compare this critical stress to the first Piola-Kirchhoff stresses obtained in the simulations. Thus, this comparison is made in the approximation of geometrically linear elasticity, in which the two Piola-Kirchhoff stress tensors and the Cauchy stress tensor are equivalent.

In Fig. 6 we plot the deviatoric stress field in the bent beam relative to the critical stress for several strengths of the applied forces at $T = 1.03T_c$. The regions where the local stress is larger than the critical stress are plotted in white/black according to its positive/negative sign. In the remaining parts of the beam the strength of the local deviatoric stress is represented using a gray scale. It is found that in the range of external forces used in Fig. 5 the local deviatoric stress is above the critical stress in large parts of the beam which is sufficient to prevent the existence of discontinuities and hysteresis in the whole system. For smaller values of the applied forces several discontinuities in the entropy curves are obtained (not shown in the figure). These may be associated with the nucleation of the rectangular phase at the center of the beam or at its ends where the curvature and thus the local stress may be very small.

From the entropy curves we have computed the isothermal entropy change of the beam when the external forces

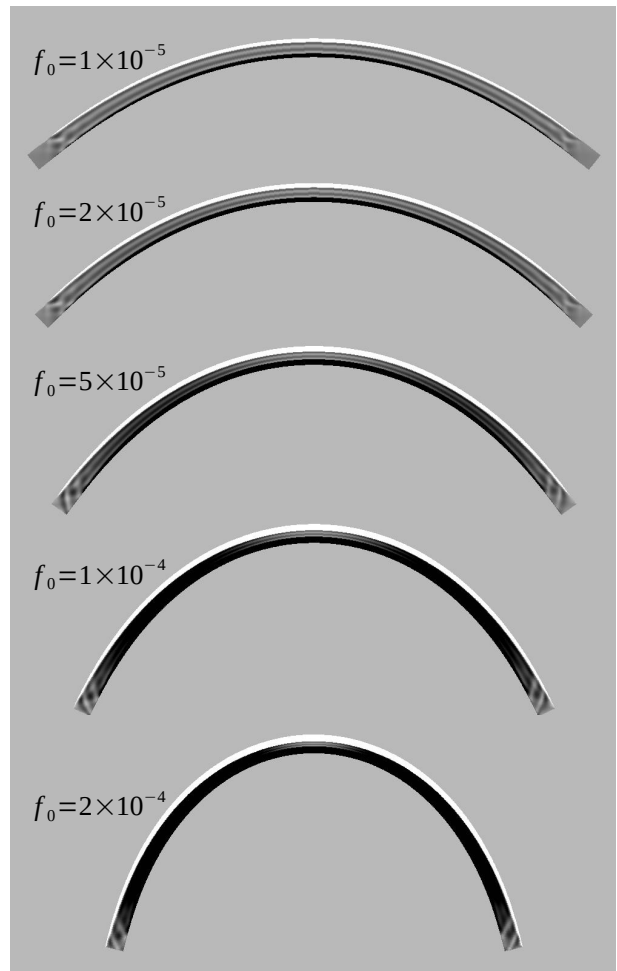


FIG. 6: Deviatoric stress field in the bent beam relative to the critical deviatoric stress. Regions with a positive/negative stress larger than the critical stress are plotted in white/black whereas in the remaining parts of the beam the local deviatoric stress is represented using a gray scale. The results correspond to $T = 1.03T_c$ for several values of the parameter f_0 , which controls the strength of the distribution of applied forces.

are applied, $\Delta S = S(f_0, T) - S(f_0 = 0, T)$ (Fig. 7). Due to the continuity of the entropy curves when the external forces are applied there is a single discontinuity in the isothermal entropy change associated with the discontinuity of the entropy curve in the absence of applied forces. This yields a temperature dependence of the isothermal entropy change that is somewhat different from the usual peak at the transition temperature. Above the transition temperature we obtain that the entropy change increases with the strength of the applied forces. In the vicinity of the phase transition the ratio between the entropy change and the strength of the applied forces is larger for small forces, and the temperature dependence of the entropy change is smaller if the applied forces are large.

We have also computed the adiabatic temperature

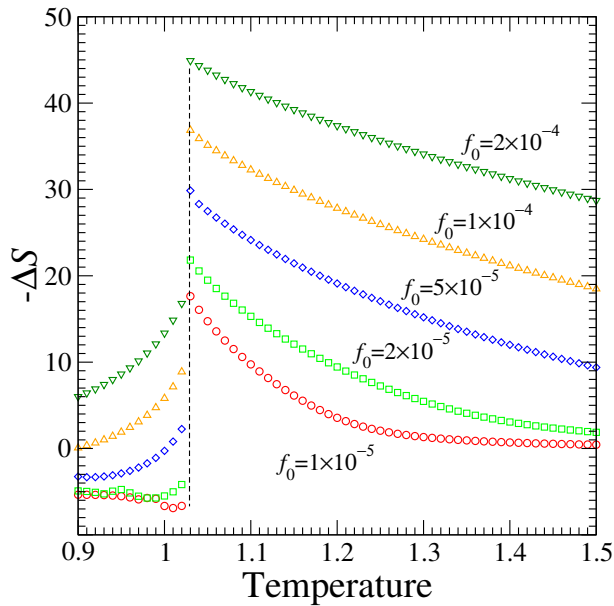


FIG. 7: Stress-induced isothermal entropy change as a function of temperature for selected values of the applied external forces from 0 to f_0 .

change as a function of the initial temperature when the external forces are applied to the beam, $\Delta T = T(f_0, S) - T(f_0 = 0, S)$. The results are shown in Fig. 8. As before, in the curves of the temperature change there

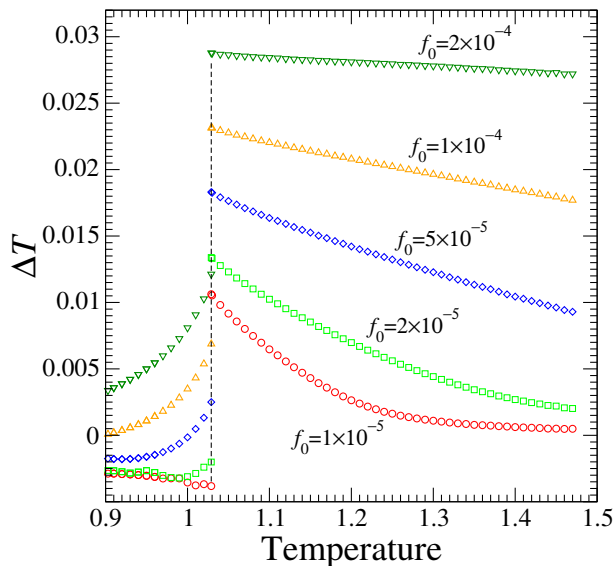


FIG. 8: Stress-induced adiabatic temperature change as a function of the initial temperature for selected values of the applied external forces from 0 to f_0 .

is a single discontinuity associated with the discontinuity of the entropy curve in the absence of applied forces. We also find that the larger the applied forces the larger the thermal response. In addition, for large forces the temperature dependence of the adiabatic temperature change

obtained above the transition temperature is very weak.

As the bending angle can be easily measured in experiments we also present the thermal response of the beam upon bending in terms of this quantity. In Fig. 9(a) we plot the isothermal entropy change of the beam at $T = 1.03T_c$ as a function of the bending angle. The

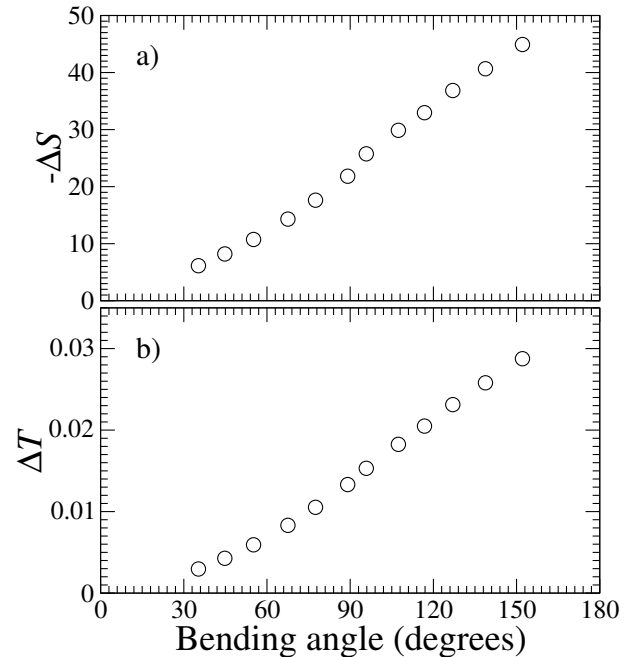


FIG. 9: Stress-induced isothermal entropy change (a) and adiabatic temperature change (b) as a function of the bending angle at $T = 1.03T_c$.

adiabatic temperature change at the same initial temperature is shown in Fig. 9(b). In both cases we obtain an almost linear behavior. This is surprising since as shown in Fig. 3 the relationship between the applied forces and the bending angle is highly nonlinear. It is also worth noting that the thermal response obtained for bending angles smaller than 30° is very small, as this bending angle can be obtained with very small forces that are insufficient to induce the phase transition. In this small force regime we obtain discontinuities in the entropy curves and hysteresis.

Considering the reduced unit of temperature that corresponds to the Fe-30.0Pd (at. %) alloy^{25,29}, $T_c = 257$ K, the average temperature change of the simulated beam for a bending angle $\theta = 60^\circ$ is $\Delta T = 1.7$ K. This result will strongly depend on the ratio L_y/L_x of the beam. Short and thick beams require large forces to be bent. On the contrary, long and thin beams can be easily bent but lead to a more localized deformation and caloric response.

The effect of the external forces on the phase transformation can be visualized by plotting the fraction of the beam that has transformed to the rectangular phase versus the bending angle. This is shown in Fig. 10 at three different temperatures. A local area of the beam is

considered to have transformed to the rectangular phase if the local deviatoric strain is larger than 50% of the transformation strain that is obtained at the transition temperature in the absence of stress, $e_2^T = 0.0206$. The

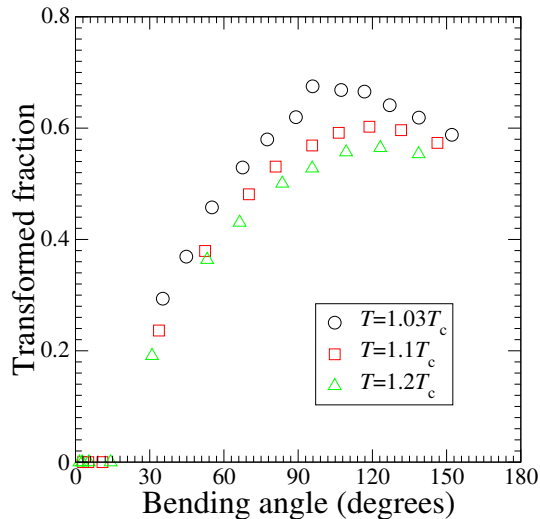


FIG. 10: Transformed fraction of the beam vs bending angle at three different temperatures.

minimum bending angle that is needed to nucleate the rectangular phase is almost independent of temperature, although the forces needed to bend the beam by such an angle increase with temperature. Once the rectangular phase nucleates the transformed fraction increases with the bending angle up to a maximum value that is reached for large bending angles ($> 90^\circ$). We expect the elastic and thermodynamic response of the beam to such large bending angles to strongly depend on how the external forces are applied.

IV. SUMMARY AND CONCLUSIONS

We have used a Ginzburg-Landau model embedded into a vibrational model to study the flexocaloric effect in a beam near a ferroelastic transition. The equilibrium strain configurations of the beam at several temperatures

and strengths of the applied forces have been obtained by solving the corresponding dynamical equations, and the associated entropy has been computed. It is found that the entropy-temperature curves are continuous for applied forces above a given threshold. This is related to the existence of a critical point in the stress-temperature phase diagram of ferroelastic materials. If the applied forces are sufficiently large the local deviatoric stress is larger than the critical stress in large parts of the beam. This leads to a reduction of the hysteresis associated with the phase transition that in small systems is completely suppressed.

The flexocaloric effect is characterized by the isothermal entropy change and the adiabatic temperature change obtained from the entropy curves¹⁻⁴. A larger thermal response relative to the applied forces is obtained at temperatures slightly above the transition temperature. The maximum caloric response is also plotted in terms of the bending angle of the beam and an almost linear relation is obtained, whereas the relation between the bending angle and the applied forces is highly non-linear. The peculiar morphology of the microstructure in the beam is found to be similar to that observed in experiments²¹.

It is also obtained that there is a minimum bending angle that is necessary to induce the nucleation of the low symmetry phase by stress. This minimum bending angle has a weak dependence on temperature. Finally, as a natural extension of the present study, it would be noteworthy to study *twistocaloric* effect in ferroelastic beams or rods subjected to a torque (or twisting strain¹¹) as well as caloric effects in flexoelectric¹⁵⁻¹⁷, flexomagnetic¹⁸, flexomagnetoelectric^{19,20} and other flexoelastic³⁰ materials.

Acknowledgments

This research was supported by CICYT (Spain) under Project No. PID2020-113549RB-I00. The work at Los Alamos National Laboratory (A.S.) was carried out under the auspices of the U.S. DOE and NNSA under Contract No. DEAC52-06NA25396.

¹ X. Moya and N. D. Mathur, *Caloric materials for cooling and heating*, Science **370**, 797–803 (2020).

² L. Mañosa, A. Planes, and M. Acet, *Advanced materials for solid-state refrigeration*, J. Mater. Chem. A **1**, 4925–4936 (2013).

³ K. A. Gschneidner Jr, V. K. Pecharsky, and A. O. Tsokol, *Recent developments in magnetocaloric materials*, Rep. Prog. Phys. **68**, 1479–1539 (2005).

⁴ A. Planes, L. Mañosa, and M. Acet, *Magnetocaloric effect and its relation to shape-memory properties in ferromagnetic Heusler alloys*, J. Phys. Cond. Matter **21**, 233201

(2009).

⁵ Y. Song, X. Chen, V. Dabade, T. W. Shield, and R. D. James, *Enhanced reversibility and unusual microstructure of a phase-transforming material*, Nature, **502**, 85–88 (2013).

⁶ L. Mañosa and A. Planes, *Materials with giant mechanocaloric effects: Cooling by strength*, Adv. Mater. **29**, 1603607 (2017).

⁷ L. Mañosa and A. Planes, *Solid-state cooling by stress: A perspective*, Appl. Phys. Lett. **116**, 050501 (2020).

⁸ F. Bruederlin, L. Bumke, C. Chluba, H. Ossmer, E.

- Quandt, and M. Kohl, *Elastocaloric cooling on the miniature scale: A review on materials and device engineering*, Energy Technol. **6** 1588–1604 (2018).
- ⁹ A. Czernuszewicz, L. Griffith, J. Slaughter, and V. Pecharsky, *Low-force compressive and tensile actuation for elastocaloric heat pumps*, Appl. Mater. Today **19**, 100557 (2020).
 - ¹⁰ D. J. Sharar, J. Radice, R. Warzoha, B. Hanrahan, and A. Smith, *Low-force elastocaloric refrigeration via bending*, Appl. Phys. Lett. **118**, 184103 (2021).
 - ¹¹ R. Wang et al., *Torsional refrigeration by twisted, coiled, and supercoiled fibers*, Science **366**, 216–221 (2019).
 - ¹² R. Wang, X. Zhou, W. Wang, and Z. Liu, *Twist-based cooling of polyvinylidene difluoride for mechanothermochromic fibers*, Chem. Engng. J. **417**, 128060 (2021).
 - ¹³ P. Zubko, G. Catalan, and A. K. Tagantsev, *Flexoelectric effect in solids*, Annu. Rev. Mater. Res. **43**, 387–421 (2013).
 - ¹⁴ Y. Li, S. P. Lin, Y. J. Wang, D. C. Ma, and B. Wang, *Bending influence of the electrocaloric effect in a ferroelectric/paraelectric bilayer system*, J. Phys. D: Appl. Phys. **49**, 065305 (2016).
 - ¹⁵ H. Khassaf, T. Patel, R. J. Hebert, and S. P. Alpay, *Flexocaloric response of epitaxial ferroelectric films*, J. Appl. Phys. **123**, 024102 (2018).
 - ¹⁶ S. Patel, *Flexocaloric effect in ferroelectric materials: methods of indirect evaluation*, Appl. Phys. A **127**, 411 (2021).
 - ¹⁷ A. S. Starkov and I. A. Starkov, *Flexocaloric effect in thin plates of barium titanate and strontium titanate*, Phys. Solid State **61**, 2542–2546 (2019).
 - ¹⁸ P. Lukashev and R. F. Sabirianov, *Flexomagnetic effect in frustrated triangular magnetic structures*, Phys. Rev. B **82**, 094417 (2010).
 - ¹⁹ A. K. Zvezdin and A. P. Pyatakov, *Flexomagnetoelectric effect in bismuth ferrite*, Phys. Stat. Solidi B **246**, 1956–1960 (2009).
 - ²⁰ A. P. Pyatakov and A. K. Zvezdin, *Flexomagnetoelectric interaction in multiferroics*, Eur. Phys. J. B **71**, 419–427 (2009).
 - ²¹ K. Otsuka, H. Sakamoto, and K. Shimizu, *A new type of pseudoelasticity in single variant twinned martensites*, Scripta Metall. **11**, 41–46 (1977).
 - ²² P. Howell, G. Kozyreff, and J. Ockendon, *Applied Solid Mechanics* (Cambridge University Press, New York, 2009).
 - ²³ C. Polizzotto, *A note on the higher order strain and stress tensors within deformation gradient elasticity theories: physical interpretations and comparisons*, Int. J. Solids Struct. **90**, 116–121 (2016).
 - ²⁴ D. C. Rapaport, *The art of molecular dynamics simulation* (Cambridge University Press, New York, 1995).
 - ²⁵ S. Kartha, J. A. Krumhansl, J. P. Sethna, and L. K. Wickham, *Disorder-driven pretransitional tweed pattern in martensitic transformations*, Phys. Rev. B **52**, 803–822 (1995).
 - ²⁶ R. Oshima, M. Sugiyama, and F. E. Fujita, *Tweed structures associated with FCC-FCT transformations in Fe-Pd alloys*, Metall. Trans. A **19A**, 803–810 (1988).
 - ²⁷ F. Xiao, T. Fukuda, and T. Kakeshita, *Critical point of martensitic transformation under stress in an Fe-31.2Pd (at. %) shape memory alloy*, Philos. Mag. **95**, 1390–1398 (2015).
 - ²⁸ H. Chen, Y. Wang, Z. Nie, R. Li, D. Cong, W. Liu, F. Ye, Y. Liu, P. Cao, F. Tian, X. Shen, R. Yu, L. Vitos, M. Zhang, S. Li, X. Zhang, H. Zheng, J. F. Mitchell, and Y. Ren, *Unprecedented non-hysteretic superelasticity of [001]-oriented NiCoFeGa single crystals*, Nature Mater. **19**, 712–718 (2020).
 - ²⁹ S. Muto, R. Oshima, and F. E. Fujita, *Elastic softening and elastic strain energy consideration in FCC-FCT transformation of Fe-Pd alloys*, Acta Metall. Mater. **38**, 685–694 (1990).
 - ³⁰ M. I. Capar, A. Nar, A. V. Zakharov, and A. A. Vakulenko, *Flexoelastic properties of polar liquid crystals*, Phys. Solid State **53**, 435–441 (2011).